THE JOURNAL OF BIOLOGICAL CHEMISTRY VOL. 286, NO. 31, pp. 27425–27435, August 5, 2011

Identification and Functional Characterization of Kir2.6 Mutations Associated with Non-familial Hypokalemic Periodic Paralysis*

Received for publication, April 10, 2011, and in revised form, June 2, 2011 Published, JBC Papers in Press, June 10, 2011, DOI 10.1074/jbc.M111.249656

Chih-Jen Cheng[‡§1], Shih-Hua Lin[§2], Yi-Fen Lo[§], Sung-Sen Yang[§], Yu-Juei Hsu[§], Stephen C. Cannon[¶], and Chou-Long Huang[‡3]

From the [‡]Department of Medicine, Division of Nephrology, and the [¶]Department of Neurology and Program in Neuroscience, University of Texas, Southwestern Medical Center, Dallas, Texas 75390-8856 and the [§]Department of Medicine, Division of Nephrology, Tri-Service General Hospital, National Defense Medical Center, Taipei 114, Taiwan

Hypokalemic periodic paralysis (hypoKPP) is characterized by episodic flaccid paralysis of muscle and acute hypokalemia during attacks. Familial forms of hypoKPP are predominantly caused by mutations of either voltage-gated Ca^{2+} or Na^+ channels. The pathogenic gene mutation in non-familial hypoKPP, consisting mainly of thyrotoxic periodic paralysis (TPP) and sporadic periodic paralysis (SPP), is largely unknown. Recently, mutations in *KCNJ18*, which encodes a skeletal muscle-specific inwardly rectifying K^+ channel Kir2.6, were reported in some TPP patients. Whether mutations of Kir2.6 occur in other patients with non-familial hypoKPP and how mutations of the channel predispose patients to paralysis are unknown. Here, we report one conserved heterozygous mutation in *KCNJ18* in two TPP patients and two separate heterozygous mutations in two SPP patients. These mutations result in V168M, R43C, and A200P amino acid substitution of Kir2.6, respectively. Compared with the wild type channel, whole-cell currents of R43C and V168M mutants were reduced by ~78 and 43%, respectively. No current was detected for the A200P mutant. Single channel conductance and open probability were reduced for R43C and V168M, respectively. Biotinylation assays showed reduced cell surface abundance for R43C and A200P. All three mutants exerted dominant negative inhibition on wild type Kir2.6 as well as wild type Kir2.1, another Kir channel expressed in the skeletal muscle. Thus, mutations of Kir2.6 are associated with SPP as well as TPP. We suggest that decreased outward K^+ current from hypofunction of Kir2.6 predisposes the sarcolemma to hypokalemia-induced paradoxical depolarization during attacks, which in turn leads to Na^+ channel inactivation and inexcitability of muscles.

Hypokalemic periodic paralysis (hypoKPP)[4] is a disorder of heterogeneous etiologies in which an abrupt onset muscle paralysis is associated with a drop in the serum potassium (K^+) level (1, 2). HypoKPP exists in familial or non-familial form. Familial hypoKPP is inherited in an autosomal-dominant pattern and is predominantly caused by mutations in genes encoding for a skeletal muscle-specific voltage-gated Na^+ channel $Na_v1.4$ (*SCN4A*) or the L-type Ca^{2+} channel $Ca_v1.1$ (*CACNA1S*) (3, 4). About 10% of cases of familial hypoKPP remain genetically undefined (5). Familial hypoKPP is more common among Caucasians (6).

One common form of non-familial hypoKPP is thyrotoxic periodic paralysis (TPP) (7). TPP has a predilection for Asian and Hispanic individuals with the incidence of ~2% in patients with hyperthyroidism (8). The incidence of TPP in non-Hispanic Caucasians is estimated at between 0.1 and 0.2% (9). The clinical presentation of muscle weakness and acute hypokalemia in patients with TPP is indistinguishable from those with familial hypoKPP. TPP can occur in association with any of the causes of hyperthyroidism. Prior history of hyperthyroidism may be absent. Although some have no overt clinical symptoms of hyperthyroidism, all TPP patients have elevated blood levels of thyroid hormones and depressed thyroid stimulating hormone (TSH) during attacks (7, 10, 11). Another relatively common form of non-familial hypoKPP, called sporadic periodic paralysis (SPP), also afflicts predominantly Asians and presents with normal blood levels of thyroid hormones and TSH during attacks.

The pathogenesis of non-familial hypoKPP remains mysterious. The phenotypic similarity between familial hypoKPP and TPP suggests defects in ion channels. Indeed, a recent study reported that mutations in *KCNJ18* gene encoding a novel member of inward rectifier K^+ channel, Kir2.6, occur in some TPP patients (12). Interestingly, the *KCNJ18* gene contains a 5′-upstream thyroid hormone response element, which is

* This work was supported, in whole or in part, by National Institutes of Health Grants DK59530 (to C.-L. H.) and P30DK079328 (UT Southwestern Medical Center O'Brien Center). This study was also supported by the National Science Council, Taiwan (NSC 93-2314-B-016-031 (to S.-H. L.)) and the Research Fund of Tri-Service General Hospital (SGH-C-93-51 (to S.-H. L.)). Functional experiments were performed by C.-J. Cheng in partial fulfillment of the requirements of the Ph.D. degree at the University of Texas Southwestern Medical Center at Dallas.

[1] Supported by a scholarship grant from the Ministry of Defense, Taiwan.

[2] To whom correspondence may be addressed: Division of Nephrology, Dept. of Medicine, Tri-Service General Hospital, No. 325, Section 2, Cheng-Kung Rd., Neihu 114, Taipei, Taiwan. Tel.: 886-2-87927213; Fax: 886-2-87927134; E-mail: l521116@ndmctsgh.edu.tw.

[3] Holds the Jacob Lemann Professorship in Calcium Transport of the University of Texas Southwestern Medical Center. To whom correspondence may be addressed: UT Southwestern Medical Center, Dept. of Medicine, 5323 Harry Hines Blvd., Dallas, TX 75390-8856. Tel.: 214-648-8627; Fax: 214-648-2071; E-mail: chou-long.huang@utsouthwestern.edu.

[4] The abbreviations used are: hypoKPP, hypokalemic periodic paralysis; TPP, thyrotoxic periodic paralysis; SPP, sporadic periodic paralysis; fT_4, free thyroxin; T_3, triiodothyronine; TSH, thyroid stimulating hormone; pF, picofarads..

important for the transcription of *KCNJ18* enhanced by thyroid hormone. It was suggested that mutations of Kir2.6 affect membrane excitability of skeletal muscle, predisposing patients to muscle paralysis, and that the transcriptional up-regulation of Kir2.6 by thyroid hormones is pivotal in the pathogenesis. In this report we investigated whether mutations of Kir2.6 occur in other non-familial hypoKPP, specifically SPP. We found heterozygous loss-of-function mutations of Kir2.6 in patients with SPP as well as patients with TPP. The mutant Kir2.6 channels exert dominant negative inhibition not only on wild type Kir2.6 but also on Kir2.1, another channel expressed in skeletal muscle. Our results support the notion that decreased outward K^+ currents predispose the sarcolemma to paradoxical depolarization during hypokalemia, a characteristic pathogenic feature underlying Na^+ channel inactivation and inexcitability of muscles in hypoKPP patients.

EXPERIMENTAL PROCEDURES

Identification of Patients with TPP or SPP—The study protocol was approved by the Ethics Committee on Human Studies at Tri-Service General Hospital in Taiwan. Written informed consent was obtained from each patient. We collected DNA and clinical and laboratory data from 120 patients with the diagnosis of TPP and 60 patients with SPP admitted to Tri-Service General Hospital or affiliated hospitals between 2002 and 2009. TPP is defined as acute muscle weakness with an inability to ambulate (muscle power less than Medical Research Council scale grade 3) accompanied by hypokalemia (plasma K^+ level less than 3.0 mEq/liter) at presentation caused by a sudden shift of K^+ into cells (urine transtubular K^+ gradient <3) and hyperthyroidism, confirmed by suppressed plasma TSH and elevated levels of plasma triiodothyronine (T_3) and free thyroxin (fT_4). Renal and intestinal K^+ wasting and medications as causes of hypokalemia were excluded based on a transtubular K^+ gradient >3 (suggesting renal K^+ wasting), no medications including diuretics, laxatives, amphetamine, β-agonist, caffeine, and no history of increased gastrointestinal output. Other identifiable causes of transcellular K^+ shift, such as fluid-electrolyte and acid-base disturbances, are also excluded. SPP is diagnosed based on no family history of episodic paralysis and fulfillment of the above criteria of hypokalemic periodic paralysis except that with normal levels of plasma T_3, fT_4, and TSH. Screening of known genes mutated in familial hypoKPP including *CACNA1S*, *SCN4A*, and *KCNJ2* were performed. Among TPP patients include in this study, we found no mutations in *CACNA1S*, *SCN4A*, and *KCNJ2*. Among SPP patients included in this study, we found one mutation in *CACNA1S* (R1239H) and three mutations in *SCN4A* (two R669H and one R1135H) (see "Discussion"). The two SPP patients carrying mutations in *KCNJ18* reported in this study (see below) do not carry any of the above mutations in *CACNA1S or SCN4A*. Blood and urine biochemical values and electrolytes were determined with the use of automated methods (AU 5000 chemistry analyzer; Olympus, Tokyo). Thyroid function tests were determined by radioimmunoassay (RIA) method.

Mutational Analysis of KCNJ18 Gene—Genomic DNA was prepared from the peripheral blood of TPP and SPP patients and healthy control subjects using the QIAamp (Qiagen). Sequencing of *KCNJ18* was performed as previously described (12). PCR primers were designed against the GenBank™ accession NM_021012 sequence with the forward primer containing two nucleotide mismatches to favor amplification of diverse products. We performed nested PCR of Kir2.6 with 20 ng of outer PCR product in a 50-μl reaction containing 10 mM Tris-HCl (pH 9 at 25 °C), 50 mM KCl, 0.1% Triton X-100, 200 μM each dNTP, 1.5 mM $MgCl_2$, 1 unit of Taq DNA polymerase, and 25 pmol of forward and reverse primers (CGAGGAGGGCGAGTACATC; CAAGATGGTGATGGGCG) under the following conditions: 5 cycles at 66 °C for 30 s and 72 °C for 1 min plus 30 cycles at 64 °C for 30 s and 72 °C for 1 min, each cycle preceded by a 94 °C step. The resulting products were subcloned into pCR2.1 (Invitrogen) and sequenced. The products were sequenced with the same primers used for amplification, with BigDye terminator v3.1 mix and subsequent analysis by capillary electrophoresis on an ABI Prism 377 Genetic analysis (PerkinElmer Life Sciences).

Plasmid DNA and Transient Expression of Kir Channels in Cultured Cells—Human embryonic kidney (HEK) 293 cells were cultured as described previously (13). Cells were transfected with wild type and/or mutant cDNA of Kir2.6 (pEGFPC2-Kir2.6, a gift from Dr. L. J. Ptacek, University of California, San Francisco) and/or Kir2.1 (in pcDNA3.1 vector) using FuGENE HD (Roche Applied Science). Point mutations were generated by site-directed mutagenesis (QuikChange kit, Stratagene) and confirmed by sequencing. To avoid saturation of channel protein expression, the maximal amount of cDNA for channels used for transfection was $\leq$0.9 μg. The total amount of plasmid DNA in each experimental group was balanced using empty vector.

Immunoblotting and Surface Biotinylation Assay—Transfected, cultured HEK cells were incubated with lysis buffer (50 mM HEPES (pH 7.6), 150 mM sodium chloride, 0.5% Triton X-100, 10% glycerol, 0.1% SDS) containing protease inhibitor mixture (Complete Mini, Roche Applied Science) and phosphatase inhibitor mixture (PhosSTOP, Roche Applied Science). After shaking 30 min on the rotator at 4 °C, extracts were clarified by centrifugation. Protein concentrations of supernatant were measured by the Bradford assay using bovine serum albumin as a standard. Equal amounts of lysates were mixed with Laemmli sample buffer and then separated by SDS-PAGE under reducing conditions. Proteins were transferred to nitrocellulose membranes, blocked by 5% nonfat milk, and incubated with the anti-GFP antibody (horseradish peroxidase conjugate; Invitrogen; 1:1000 dilution) to detect protein expression of pEGFP-Kir2.6. Anti-β-actin antibody was used to detect endogenous β-actin as a loading control. Bound antibodies were detected using ECL detection reagent (Pierce).

For biotinylation of cell-surface Kir2.6, transfected HEK cells (per 35-mm well) were washed with 1 ml of ice-cold PBS three times and incubated with 1 ml of PBS containing 1.5 mg/ml EZ-link-NHS-SS-biotin (Thermo Scientific) for 2 h at 4 °C. After quenching with glycine-containing PBS for 20 min, cells were lysed in a radioimmune precipitation assay buffer (150 mM NaCl, 50 mM Tris-HCl, 5 mM EDTA, 1% Triton X-100, 0.5% deoxycholate, and 0.1% SDS) containing protease inhibitor mixture for 30 min. Biotinylated proteins were precipitated by

streptavidin-agarose beads (Thermo Scientific) for 2 h at 4 °C. Beads were subsequently washed 3 times with TBS containing 1% Triton X-100. Biotin- labeled proteins were eluted in sample buffer, separated by SDS-PAGE, and transferred to nitrocellulose membranes for Western blotting using anti-GFP antibody. Biotinylation experiment was performed four times with similar results.

Electrophysiological Recording—About 36–48 h after transfection, cells were trypsinized and plated on poly-L-lysine coated coverslips. Whole cell Kir2.x currents were recorded by using an Axopatch 200B amplifier (Axon Instruments, Foster City, CA) as previously described (13). The pipette resistance was around 2–4 megaohms. Transfected cells were identified by green fluorescence using epifluorescent microscopy. In whole-cell current recordings, the pipette solution contained 110 mM potassium gluconate, 20 mM KCl, 10 mM EGTA, 2 mM Mg-ATP, 5 mM glucose, 10 mM HEPES (pH 7.4); the bath solution contained 117 mM NaCl, 30 mM KCl, 1 mM $MgCl_2$, 2 mM $CaCl_2$, 10 mM HEPES (pH 7.3), 2 mM $NaHCO_3$, and 5 mM glucose. The cell membrane capacitance and series resistance were monitored and compensated (>75%) electronically. The voltage protocol consisted of a 0-mV holding potential for 50 ms and 100-ms steps from −60 to 60 mV in 10-mV increments. After the initial recording of current, $BaCl_2$ (30 μM) was added to the bath solution to inhibit K^+-specific currents. Residual current in the presence of Ba^{2+} was subtracted from the total current. Data were sampled at 5 kHz with a 2-kHz low pass filter. ClampX 9.2 software (Axon Instruments) was used for data acquisition. Current density was calculated by dividing current at the designated holding potential (pA; measured at 25 °C) by capacitance (pF). Results were shown as the means ± S.E. ($n = 6–10$). Each experiment (*i.e.* set of results shown in each panel of a figure) was repeated two to four times. For cell-attached single-channel recordings, pipette and bath solution each contained 150 mM KCl, 2 mM $MgCl_2$, 1 mM EGTA, and 10 mM HEPES (pH 7.4). Currents were recorded at 50 kHz continuously for 1–10 min at the test voltage from 120 to −120 mV with a 1-kHz low pass filter. Single-channel current were calculated by curve-fitting the sum of a number of Gaussian curves to the recorded data. Open probability was calculated from the relative areas of these Gaussian curves. Single channel conductance was calculated from the slope of single-channel current amplitudes between −40 and −120 mV.

Statistical Analysis—Clinical and laboratory data of patients were presented as the mean ± S.D. Two-tailed unpaired Student's *t* test was used to compare the differences among TPP and SPP. In electrophysiological and biotinylation experiments, data analysis and curve-fitting were performed with the Prism (Version 5.03) software (GraphPad Software, San Diego, CA). Data were presented as the mean ± S.E. Statistical comparisons between two groups of data were made using two-tailed unpaired Student's *t* test. Multiple comparisons were determined using one-way analysis of variance. Statistical significance was defined as *p* values less than 0.05 for single comparison and less than 0.01 for multiple comparisons.

TABLE 1
Clinical and laboratory characteristics of TPP and SPP patients

	TPP	SPP
Number	120	60
Age	29 ± 6	25 ± 8
Male:Female	116:4	60:0
Plasma		
K^+ (3.5–5.1 mEq/liter)	2.1 ± 0.2	2.2 ± 0.2
T_3 (86–187 ng/dl)	334 ± 91[a]	124 ± 30
fT_4 (0.8–2.0 ng/dl)	4.0 ± 1.1[a]	1.1 ± 0.4
TSH (0.35–5.0 μU/liter)	<0.03[a]	2.3 ± 1.0
Na^+ (136–142 mEq/ iter)	141 ± 2	142 ± 5
Cl^- (98–106 mEq/liter)	106 ± 2	103 ± 8
Phosphate (2.6–4.6 mg/dl)	2.0 ± 0.5[a]	2.6 ± 0.7
Ionized calcium (4.5–5.3 mg/dl)	4.8 ± 0.2	4.7 ± 0.2
Magnesium (1.7–2.4 mg/dl)	1.8 ± 0.3	2.0 ± 0.4
Urea nitrogen (12–20 mg/dl)	12 ± 3	12 ± 6
Creatinine (Cr) (0.7–1.2 mg/dl)	0.7 ± 0.2[a]	1.0 ± 0.3
Urine		
K^+ (mEq/liter)	9 ± 4	11 ± 5
Creatinine (mg/dl)	108 ± 32	112 ± 37
TTKG	2.4 ± 0.9	2.1 ± 0.4

[a] $p < 0.05$.

RESULTS

Clinical and Laboratory Characteristics of TPP and SPP Patients—We studied 120 patients with the diagnosis of TPP and 60 patients with SPP. Identification and the diagnostic criteria for the patients were described under "Experimental Procedures." As shown in Table 1, the mean age of TPP and SPP patients at diagnosis were similar. The male to female ratio was 116:4 and 60:0 for TPP and SPP, respectively. Thyroid function tests including T_3 and fT_4 were markedly elevated in patients with TPP but normal in SPP. Consistent with the elevated thyroid hormone function, TSH was suppressed in patients with TPP. Both groups of patients had ictal hypokalemia. The plasma K^+ concentrations, however, were not different between two groups. As reported previously (7), plasma phosphate concentration during attacks was significantly lower in TPP than SPP, presumably reflecting a transcellular shift of phosphate stimulated by thyroid hormones. The spot urine K^+ concentration and transtubular K^+ gradient were very low in the presence of hypokalemia, consistent with the idea that an increased shift of K^+ into cells was responsible for the hypokalemia in these patients. As described under "Experimental Procedures," other causes of hypokalemia for these patients, including medications, renal, and intestinal K^+ wasting, were excluded.

Identification of Kir2.6 Mutations in Patients with TPP and SPP—In the TPP cohort, 2 of 120 patients carried the same V168M mutation. A heterozygous guanine to adenosine single-base substitution at nucleotide 502 (G502A, GTG to ATG) in exon 3 resulted in a missense mutation from valine to methionine at codon 168 (V168M) in the second transmembrane domain (Fig. 1, *A* and *B*). The thyroid function tests of these two TPP patients were as follows: free T_4, 2.92 and 6.21 ng/dl; T_3, 236 and 334 ng/dl, respectively, TSH both <0.03 IU/liter. In the SPP cohort, 2 of 60 SPP patients had different mutations in Kir2.6. A heterozygous cytosine to thymine substitution at nucleotide 127 (C127T, CGC to TGC) in exon 1 resulted in a missense mutation from arginine to cysteine at codon 43 (R43C) in the N-terminal cytoplasmic domain (Fig. 1, *A* and *B*). Another heterozygous guanine to cytosine substitution at

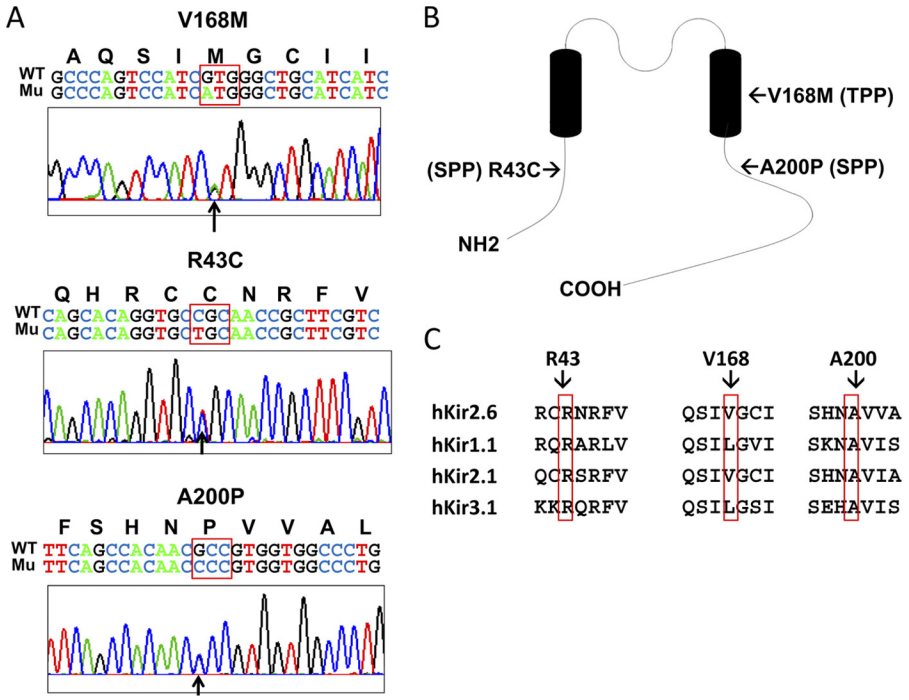

FIGURE 1. ***KCNJ18* mutations in TPP and SPP patients.** *A*, chromatograms of partial sequences of *KCNJ18* showing one heterozygous point mutation with guanine 501 mutated to adenosine (GTG → ATG), leading to a single amino acid substitution from valine to methionine (V168M), was found in two TPP patient (26- and 32-year-old males), one heterozygous point mutation with cytosine 127 mutated to thymidine (CGC → TGC), leading to the substitution of arginine 43 by cysteine (R43C), was found in a SPP patient (24-year-old male), and one heterozygous point mutation with guanine 598 mutated to cytosine (GCC → CCC), leading to alanine 200 to proline (A200P) mutation, was found in another SPP patient (52-year-old male). *Bold letters above the nucleotide sequence* represent corresponding coding amino acids. Mutated nucleotides are pointed by *arrows*, and mutated codons are surrounded by a *red box*. *WT* and *Mu* designate wild type allele and mutant allele respectively. *B*, membrane topology of Kir2.6 shows the relative locations of mutations. *C*, amino acid sequence alignment of three mutation sites from each of the four members of the inward rectifying K^+ channels is shown. Mutations are indicated by *red rectangles*.

nucleotide 598 (G598C, GCC to CCC) in exon 3 led to a missense mutation from alanine to proline at codon 200 (A200P) in the C-terminal cytoplasmic domain (Fig. 1, *A* and *B*). The thyroid function tests for these two SPP patients are as follows: free T_4, 1.21 and 1.56 ng/dl; T_3, 102 and 125 ng/dl; TSH, 3.1 and 2.3 IU/liter. Amino acids Arg-43, Val-168, and Ala-200 of Kir2.6 are identical or relatively conserved among Kir channel families (Fig. 1*C*). None of 100 healthy control subjects had these three mutations in Kir2.6.

Mutations in Kir2.6 Cause Reduced Currents—To investigate the functional impact of these mutations in the Kir2.6 channel, we measured K^+ currents through these mutant channels by ruptured whole-cell patch clamp recordings (Fig. 2*A*). To reduce endogenous Cl^- currents, we used bath and pipette solutions containing 30 mM KCl and 20 mM KCl plus 110 mM potassium gluconate, respectively. Wild type and three mutant channels expressed a similar amount of proteins in transfected HEK cells (Fig. 2*B*). The current-voltage relationship showed that K^+ currents through Kir2.6 channels were strongly inwardly rectifying with negative slopes for outward currents at membrane potentials more depolarized than −10 mV (Fig. 2*C*). Wild type and mutant Kir2.6 currents reversed at ~−23 mV, in agreement with the expected value for E_k (see Fig. 2*A* and the discussion in the legend). Compared with that for wild type Kir2.6, cells transfected with R43C and V168M mutants displayed reduced currents (Fig. 2*C*). Current density in cells expressing A200P mutant were not significantly different from mock-transfected cells (−0.9 ± 0.3 pA/pF *versus* −0.8 ± 0.2 pA/pF at −60 mV for mock-transfection), indicating that A200P mutation in Kir2.6 resulted in a complete loss-of-function. R43C and V168M mutations affected both inward and outward currents. Compared with wild type, inward currents through R43C and V168M mutants measured at a holding potential of −60 mV were reduced by ~82 and ~40%, respectively (Fig. 2*D*). Outward currents measured at a holding potential of −20 mV were reduced by ~74 and ~46%, respectively (Fig. 2*E*). Thus, mutations of Kir2.6 in patients with TPP and SPP result in reduced function or non-function of the channel.

Disease Mutations in Kir2.6 Impair Membrane Trafficking—We investigated whether these disease mutations alter cell surface abundance of Kir2.6 channels. In preliminary experiments, we found that wild type Kir2.6 protein was barely detectable by cell surface biotinylation, likely due to the fact that there is no amine group in the extracellular loop of Kir2.6 available for biotinylation. To overcome this problem, we mutagenized histidine 118 of Kir2.6, which is located in the pre-selectivity filter "turret" region of the extracellular loop and not conserved among Kir2.x families, to a lysine. Fig. 3*A* showed that H118K mutation did not affect protein expression or whole-cell current density of the "normal" and disease Kir2.6 mutants (*i.e.* whole-cell current density of H118K mutant was not significantly different from that of wild type, and current density of double mutants carrying H118K and each of the three disease mutations relative to H118K were not significantly different from results in Fig. 2*D*).

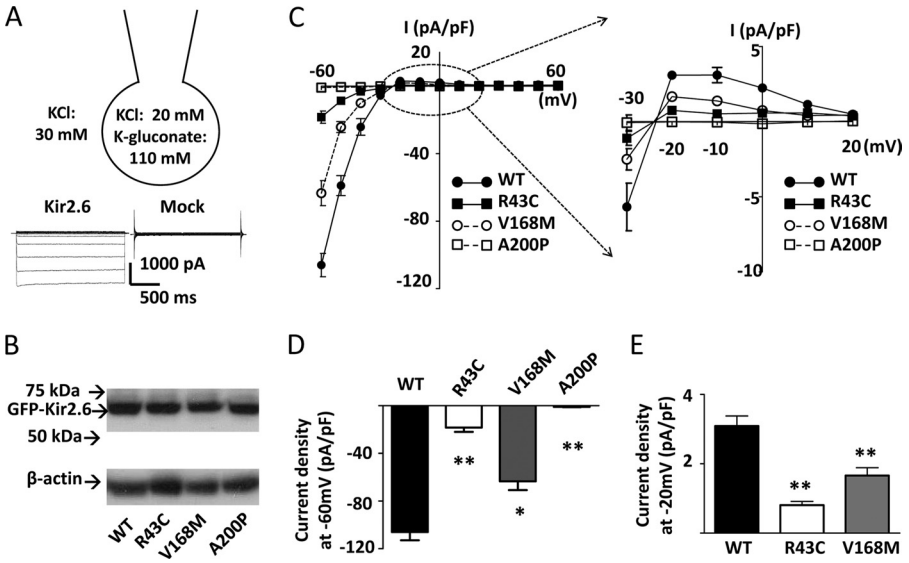

FIGURE 2. **Functional characteristics of R43C, V168M, and A200P *KCNJ18* mutations.** *A*, configuration of ruptured whole-cell recording, voltage clamp protocol (from −60 to 60 mV with 10-mV increment), and representative currents from Kir2.6- and mock-transfected cells are shown. The bath and pipette solutions contained 30 mM KCl and 20 mM KCl plus 110 mM potassium gluconate, respectively. The activity of K^+ in potassium gluconate is estimated to be ~46% that in KCl (based on the result that currents reverse at 0 mV when bath and pipette solutions contain 70 mM KCl and 20 mM KCl plus 110 mM potassium gluconate, respectively; not shown). Thus, under 30 mM KCl in the bath and 20 mM KCl plus 110 mM potassium gluconate in the pipette, the reversal potential for K^+ (E_k) is estimated at −22 mV. *B*, protein expression of WT and three mutant (R43C, V168M, A200) GFP-tagged Kir2.6 channels (GFP-Kir2.6) was detected by Western blot. β-Actin was used as a loading control. *C*, the current-voltage (*I-V*) relationship curve of WT and mutant Kir2.6 channels are shown. Currents shown are after subtraction of residual currents in the presence of 30 μM Ba^{2+}. The portion of outward hump current in this *I-V* curve was magnified (*dotted circle*, in the range of holding potential from −30 to 20 mV) to the right. *D* and *E*, shown are representative *bar graphs* of wild type and three mutant Kir2.6 current densities (pA/pF; normalized to the cell surface area) at holding potential −60 mV (*D*, inward current) or −20 mV (*E*, outward current) (mean ± S.E., $n \geq 6$ for each). The *single* and *double asterisks* denote $p < 0.05$ and $p < 0.01$, respectively, between wild type and each mutation by unpaired two-tailed Student's *t* test.

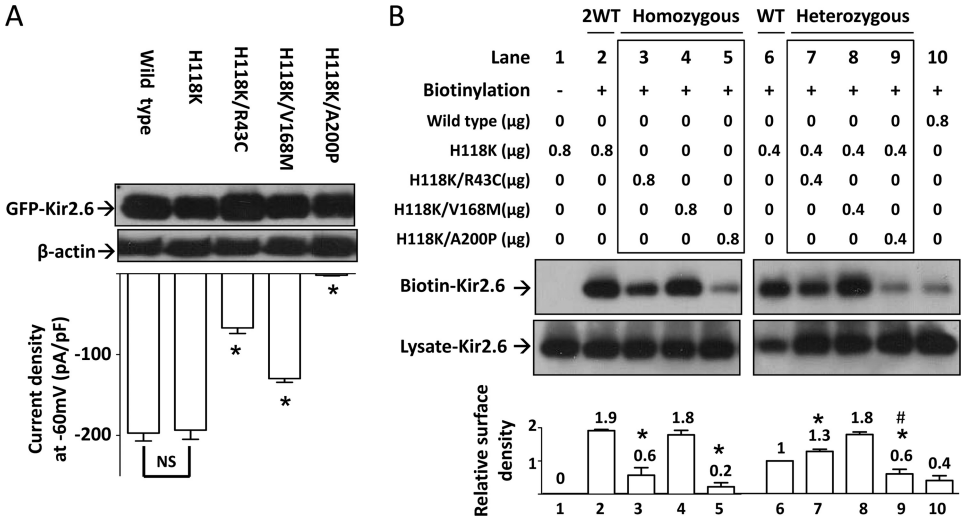

FIGURE 3. **Cell surface abundance of mutant Kir2.6 channels.** *A*, shown is the effect of H118K mutation on wild type and three mutant Kir2.6 channels. *Upper*, protein expression of wild type and mutant Kir2.6 channels was detected by Western blotting analysis. β-Actin was used as a loading control. *Lower*, Kir2.6 inward current density at a holding potential −60 mV was measured and is presented as a *bar graph* (mean ± S.E., $n \geq 6$ for each). The *asterisk* denotes $p < 0.01$ between H118-Kir2.6 and each double mutant channel. *NS* denotes not statistically significant. *B*, shown is the effect of three human Kir2.6 mutations on membrane abundance of channel. HEK cells were transfected with wild type and/or mutant Kir2.6 cDNAs (in μg of cDNA as indicated). *2WT* (*lane 2*) and *WT* (*lane 6*) reflect the ratio of protein expression from two or single allele of *KCNJ18*, respectively. Homozygous (*lane 3–5*) and heterozygous groups (*lane 7–9*) (marked by a *box*) stand for homozygous mutation with two mutant alleles and heterozygous mutation with one mutant allele and one wild type allele, respectively. *Lane 1* is a non-biotinylated group for negative control. *Lane 10* shows low efficiency of the biotinylation reaction in wild type Kir2.6. *Lysate-Kir2.6* and *Biotin-Kir2.6* represent Kir2.6 channels in HEK cell lysates and in the eluate from a mixture of HEK cell lysates and streptavidin-agarose beads, respectively. The *bar graph* at the *bottom* is the relative surface density of Kir2.6 channel (normalized to *lane 6*). The mean ± S.E. from four separate experiments is shown on the *top of each bar*. *Asterisks* denote $p < 0.01$ each group *versus lane 2*. # denotes $p < 0.01$ in *lane 9 versus lane 6*. The gel shown is representative of four experiments with similar results. The abundance of each band in the gel was measured by densitometry by the Image J program available at the NIH website.

The results of biotinylation experiments using H118K as the backbone showed that R43C and A200P mutants had significantly less surface abundance than wild type (Fig. 3*B*, *lanes 3* and *5 versus lane 2*), but V168M mutant was not different from wild type (*lane 4 versus lane 2*). To recapitulate patients who are heterozygous for the mutation, we coexpressed equal amounts of wild type and each mutant Kir2.6 cDNA and examined the amount of surface Kir2.6. Under these heterozygous condi-

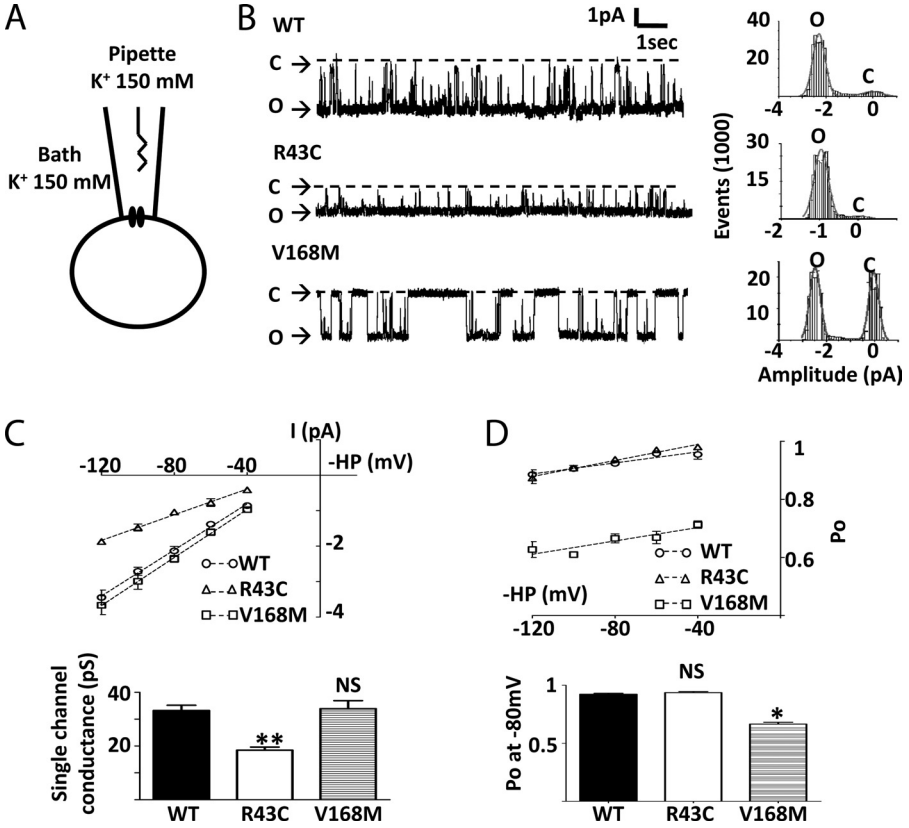

FIGURE 4. **Single channel properties of wild type and mutant Kir2.6 channels.** *A*, configuration of cell-attached single channel recording of Kir2.6 is shown. *B*, *left*, representative tracings are shown of WT (*upper*), R43C (*middle*), and V168M (*lower*) Kir2.6 single channel recording at membrane potential −80 mV. The *dotted line* indicates channel closed. *O* and *C* indicate open and closed state, respectively. *Right*, shown is an all-point histogram of the representative tracings. Bin width = 0.1 pA. *Curve lines* indicate fits by the sum of two Gaussian distributions. *C*, *upper*, single channel current-voltage (*I-V*) relationship is shown. Single channel currents were recorded at membrane holding potentials (*HP*) ranging from −40 to −120 mV. Slope conductances (*dotted line*) were calculated by linear regression. *Lower*, shown is a *bar graph* of single channel conductance. *D*, *upper*, open channel probability (P_o) of WT and mutant single channels were analyzed by an amplitude histogram at holding potentials ranging from −40 to −120 mV. *Dotted lines* were linear regressions of P_o. *Lower*, shown is a *bar graph* of open channel probability of WT and mutants at membrane potential −80 mV. *Single* and *double asterisks* denote $p < 0.05$ and $p < 0.01$, respectively, between wild type and each mutation. *NS* denotes statistically not significant.

tions, cell surface abundance of R43C and A200P mutants remained significantly lower than wild type (*lanes 7* and 9 *versus lane 2*). Interestingly, the A200P mutant exerted a dominant negative inhibition on the surface abundance of the wild type channel (*lane 9 versus lane 6*). *Lanes 1* and *10* show negative controls for biotinylation (no biotinylation reagents added) and inefficient biotinylation of the wild type channel (lacking H118K mutation), respectively. As protein expression for wild type and disease mutants are similar (Figs. 2*B* and 3*A*), the effects of R43C and A200P mutations on cell surface abundance likely represent defects in the forward membrane trafficking and/or endocytosis of the channel.

R43C and V168M Mutations Affect Single Channel Properties of Kir2.6 Channel—The effects of disease mutations on the conductance and open probability of the channel were examined using cell-attached single channel recording (Fig. 4*A*). Fig. 4*B* shows representative single channel recordings of wild type, R43C, and V168M Kir2.6 channels with symmetrical 150 mM K^+ in the pipette and bath solution and at −80-mV membrane potential (=−pipette holding potential). As shown, wild type Kir2.6 was constitutively active with a relatively high open probability over the displayed time scale (*upper tracing*). Compared with wild type, R43C (*middle tracing*) and V168M mutant (*lower tracing*) exhibited lower single-channel current amplitude and lower open probability, respectively. The single channel slope conductance was measured from a linear fit of the current-voltage relation between −40 and −120 mV (Fig. 4*C*). The R43C mutation reduced the slope conductance by 45% (33.2 ± 2.0 picosiemens (pS) for wild type *versus* 18.4 ± 1.2 pS for R43C, $n = 3$ for each, $p < 0.05$), whereas the V168M mutation had no effect on the slope conductance. We analyzed the single channel open probability of wild type and mutant channels between −40 and −120 mV membrane potentials (Fig. 4*D*). For all channels, there was a slight increase in the open probability from −120 to −40 mV. Over this voltage range, V168M mutant, but not R43C mutant, showed a lower open probability than wild type (for example, 0.67 ± 0.02 for V168M *versus* 0.92 ± 0.02 for wild type, at −80 mV, $n = 3$ each, $p < 0.01$). In conclusion, the R43C and V168M mutations in Kir2.6 reduce single-channel conductance and open probability, respectively.

Disease Mutants Exert Dominant Negative Inhibition on Wild Type Kir2.6—To better understand the *in vivo* impact of these heterozygous mutations, we examined potential dominant negative effects of mutants on wild type channel. In these experiments we cotransfected HEK cells with wild type and/or mutant Kir2.6 cDNA at the indicated concentrations (0–0.9 μg). As shown in Fig. 5*A*, current density in cells coexpressing

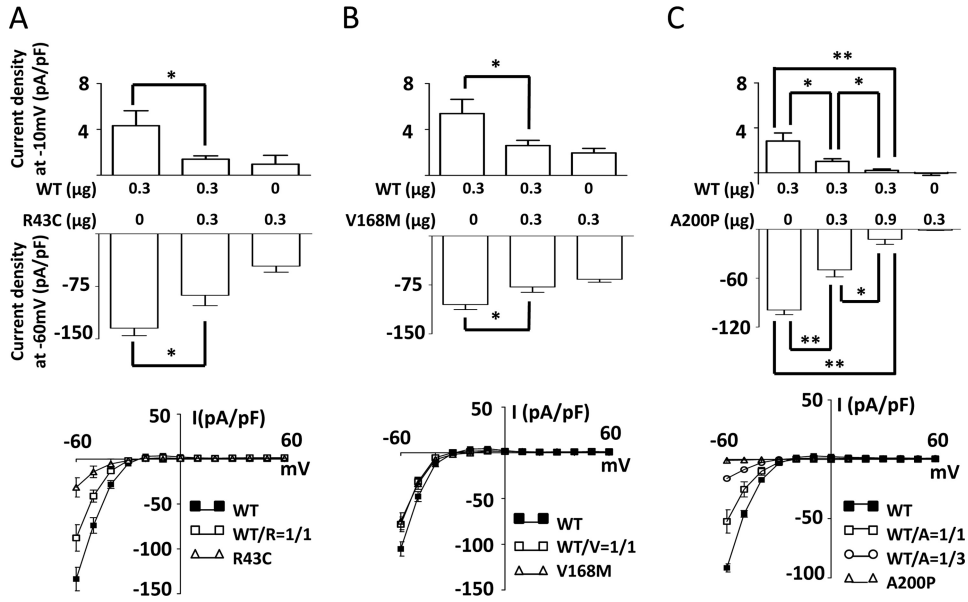

FIGURE 5. **Dominant negative effects of mutant Kir2.6 on wild type Kir2.6.** *A*, *B*, and *C*, shown is the dominant negative effect of three individual mutations on wild type Kir2.6 current. WT and mutant pEGFP-Kir2.6 cDNAs (in μg as indicated) were cotransfected into HEK cells to test the dominant negative effect of R43C (*A*), V168M (*B*), and A200P (*C*) on WT Kir2.6 current. *Upper*, the *bar graph* shows whole-cell outward (at membrane potential −10 mV) and inward current density (at membrane potential −60 mV) for wild type Kir2.6 and/or mutant Kir2.6 channels (mean ± S.E., $n \geq 6$ for each). Lower figures display current-voltage (*I-V*) relationship curves for each group (mean ± S.E., $n \geq 6$ for each). *WT/R*, *WT/V*, and *WT/A* denote the expressed protein ratio of wild type *versus* R43C, V168M, or A200P mutants, respectively (for example, WT/A = 1/3 indicates the ratio of wild type Kir2.6 channel *versus* A200P Kir2.6 channel is 1:3). *Single* and *double asterisks* denote $p < 0.05$ and $p < 0.01$ respectively between indicated groups.

R43C mutant and wild type channel subunits was significantly reduced compared with that with expression of wild type channel subunits, indicating that R43C mutant subunits exerted dominant negative inhibition on the wild type channel. Similarly, current density was reduced by coexpression with V168M or A200P (Fig. 5, *B* and *C*), indicating dominant negative inhibition of wild type channel by V168M and A200P, respectively. Interestingly, despite the relatively low cell surface expression (see Fig. 3*B*), the A200P mutant exerted a significant dominant negative inhibition on wild type even when transfected at 1:1 ratio (Fig. 5*C*, 0.3 μg of WT + 0.3 μg of A200P). This observation may be explained if incorporation of one A200P subunit is sufficient to render tetrameric channels non-functional. Consistent with the idea of dominant negative inhibition by A200P mutant, increasing the ratio of A200P to wild type to 3:1 caused further inhibition of wild type (Fig. 5*C*, 0.3 μg of WT + 0.9 μg of A200P).

Kir2.6 Forms Heteromultimers with Kir2.1 and Kir2.6 Mutants Exert Dominant Negative Inhibition on Kir2.1—The Kir2.1 channel is also expressed in skeletal muscle and reportedly forms heteromultimers with Kir2.6 (14). We thus compared Kir2.1 and Kir2.6 channel properties and explored potential interactions between disease mutant Kir2.6 and wild type Kir2.1. Current density was higher for cells expressing Kir2.1 compared with Kir2.6 when transfected with the same amount of cDNA for each (Fig. 6, *A* and *B*). Moreover, the characteristics of currents through Kir2.1 and Kir2.6 were different. As shown in the *bar graph* (Fig. 6*A*) and *I-V* relationship curves (Fig. 6*B*), Kir2.1 passed relatively more outward current than Kir2.6 at membrane potentials above the equilibrium, giving a more prominent outward "hump-shaped" current relative to Kir2.6. This difference in the *I-V* relationship is better illustrated in the *inset* of Fig. 6*A*, where Kir2.6 currents are normalized to Kir2.1. Thus, the rectification ratio, defined herein as inward current at −60 mV over outward current at −10 mV, was 6.7 for Kir2.1 and 33 for Kir2.6, respectively. We next examined K^+ currents in cells coexpressing Kir2.1 and Kir2.6. Cotransfection with cDNA for Kir2.1 and Kir2.6 (0.2 μg each) produced currents of much lower amplitude than in cells transfected with Kir2.1 alone (Fig. 6*A*; inward and outward current density were −126 and 6.8 pA/pF, respectively, for cotransfection *versus* −237 and 38.4 pA/pF, respectively for Kir2.1 alone). The rectification ratio for cotransfection was 18.5, a value between that for Kir2.1 alone (*i.e.* 6.7) and for Kir2.6 alone (*i.e.* 33). Cotransfecting an increased amount of Kir2.6 DNA (0.6 μg) further increased the rectification ratio to 31.5, a value similar to that for transfection of Kir2.6 alone (*i.e.* 33). These results support the idea that Kir2.1 and Kir2.6 can form functional heteromultimers at the cell surface.

We examined the potential effects of dominant negative inhibition on Kir2.1 by disease Kir2.6 mutants. Cotransfection of A200P mutant with Kir2.1 at 1:1 and 1:3 Kir2.1 to A200P cDNA ratios caused a dose-dependent inhibition of Kir2.1 current (Fig. 6*C*; for example, inward current density was −277, −100, and −20 pA/pF for 0, 0.2, and 0.6 μg of A200P cDNA, respectively). For comparison, coexpression of a non-functional Kir2.6 mutant carrying a glycine to alanine mutation within the GYG-selective filter at the 1:1 mutant to Kir2.1 ratio (Fig. 6*C*, *last bar highlighted by the box labeled GA*) caused inhibition of Kir2.1 currents in the magnitude similar to that exerted by A200P at a 3:1 ratio to Kir2.1 (Fig. 6*C*, *fourth bar from the left*). These results again reflect that A200P has reduced cell-surface expression (Fig. 3*B*), and a larger amount of cDNA is required for the near complete inhibition of Kir2.1.

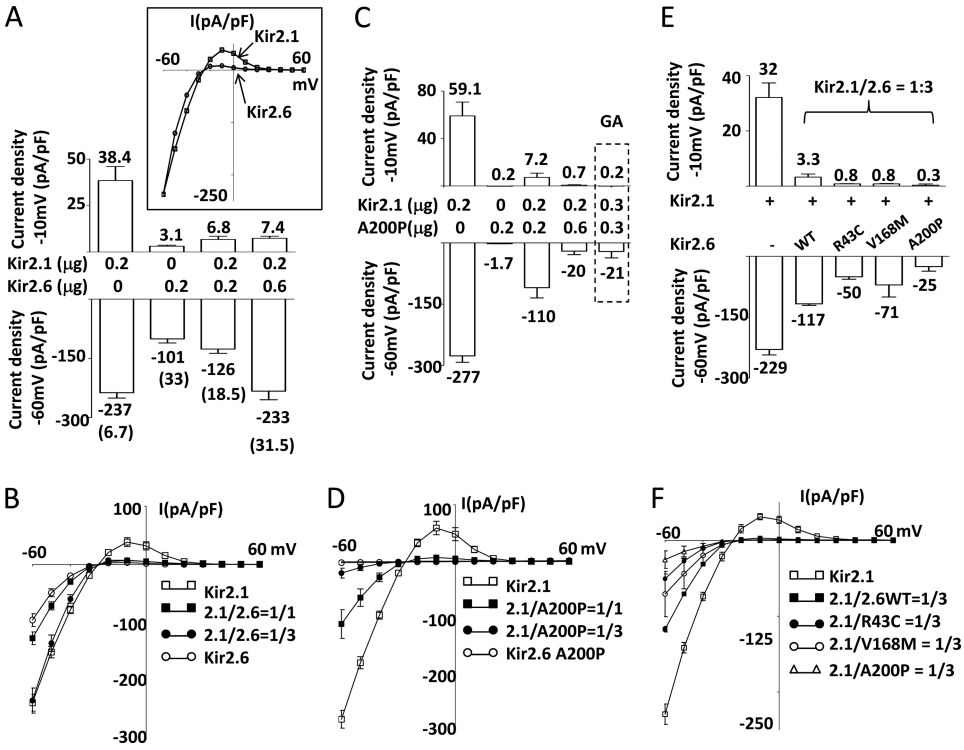

FIGURE 6. **Formation of functional heteromultimers between Kir2.1 and Kir2.6 and disease mutant Kir2.6 exerts dominant negative inhibition on Kir2.1.** *A* and *B*, currents and *I-V* relationships of homomeric and heteromeric Kir2.1 and Kir2.6 channels are shown. *C*, dose-dependent dominant negative effect of A200P Kir2.6 mutant on Kir2.1 is shown. *E*, the dominant negative effect of disease mutant Kir2.6 on Kir2.1 is shown. Kir2.1 and either wild type Kir 2.6 (*A*) or A200P Kir2.6 (*C*) (in μg of cDNA as indicated) were cotransfected in HEK cells. In *E*, the cDNA ratio of Kir2.1 *versus* either WT or disease mutant (R43C, V168M, A200P) Kir2.6 are all 1/3 (Kir2.1, 0.15 μg; Kir2.6, 0.45 μg). *Upper* and *lower bar figures* represent outward current densities at a pipette holding potential of −10 mV and inward current densities at a pipette holding potential −60 mV, respectively (mean ± S.E., $n \geq 6$ for each group). *Numbers above* or *below* each *bar* represent the mean current for each group. *Numbers in parentheses* in A indicate the absolute value of the ratio between inward current at −60 mV and outward current at −10 mV for each group. The *inset* in *A* shows the overlap of normalized current voltage (*I-V*) relationships curves of Kir 2.1 and wild type Kir2.6. The *dotted box* in *C* represents a separate experiment with Kir2.1 and G145A (*GA*) Kir2.6 cotransfected in HEK cells. *B*, *D*, and *F*, shown are current voltage (*I-V*) relationships curves of each group in *A*, *C*, and *E*, respectively. *2.1/2.6WT* and *2.1/A200P*, *2.1/R43C*, or *2.1/V168M* denote the cDNA ratio (for example, 2.1/2.6 = 1/1 indicates that the same amounts of Kir2.1 and wild type Kir2.6 cDNA were cotransfected), respectively.

Fig. 6*D* shows *I-V* relationships for experiments in Fig. 6*C*. We next examined the effects of R43C and V168M Kir2.6 mutants on wild type Kir2.1. Cells coexpressing R43C or V168M mutant and Kir2.1 at a 3:1 cDNA ratio (Fig. 6*E*, *third* and *fourth bar* from the *left*, respectively) had currents smaller than cells expressing Kir2.1 alone (*first bar* from the *left*) or cells coexpressing wild type Kir2.6 and Kir2.1 (*second bar* from the *left*), indicating that R43C and V168M mutants also exert dominant negative inhibition on Kir2.1. Fig. 6*F* shows *I-V* relationships for experiments in Fig. 6*E*.

DISCUSSION

The pathogenesis of non-familial hypoKPP remains elusive. Ryan *et al.* (12) recently reported that mutations of a skeletal muscle-specific Kir2.6 channel occur in patients with TPP. In this study we report three novel mutations of Kir2.6 in patients with SPP as well as patients with TPP. The mutations we identified in patients with TPP and SPP are heterozygous, missense substitutions of amino acids (R43C, V168M, and A200P) that result in partial or complete loss of function of Kir2.6. Among these, R43C mutation decreases single channel conductance as well as cell-surface expression of the channel protein. V168M mutation decreases single channel opening probability. A200P mutation results in non-functional channel and additionally reduces cell-surface expression of the channel protein. All disease Kir2.6 mutants exert dominant negative mutations on wild type Kir2.6 and Kir2.1, both of which play an important role in regulating resting membrane potentials of skeletal muscle. These results provide important insights into the mechanism of pathogenesis of hypoKPP.

It has been known for more than a decade that mutations of skeletal muscle voltage-gated Ca^{2+} channel $Ca_v1.1$ or Na^+ channel $Na_v1.4$ cause familial hypoKPP. The majority of mutations in $Ca_v1.1$ or $Na_v1.4$ occur in the S4 voltage sensors, changing positively charged amino acids to uncharged (5). One hallmark of hypoKPP is paradoxical depolarization of the sarcolemma induced by hypokalemia during attacks, which is believed to be a central mechanism of Na^+ channel inactivation and, thus, inexcitability of muscle. How mutations of cationic amino acids in the voltage sensor cause the paradoxical depolarization of sarcolemma during hypokalemia, however, had been an enigma. Recent studies showing that mutations in the voltage sensor create an aberrant conducting pore ("gating pore") that allows passage of small cations (Na^+ and H^+) at hyperpolarized resting membrane potentials (15, 16) provide a mechanistic explanation for paradoxical depolarization of sarcolemma during hypokalemic attacks.

The resting membrane potential (E_r) of cells is determined by the balance between outward (I_o) and inward (I_i) current (Fig.

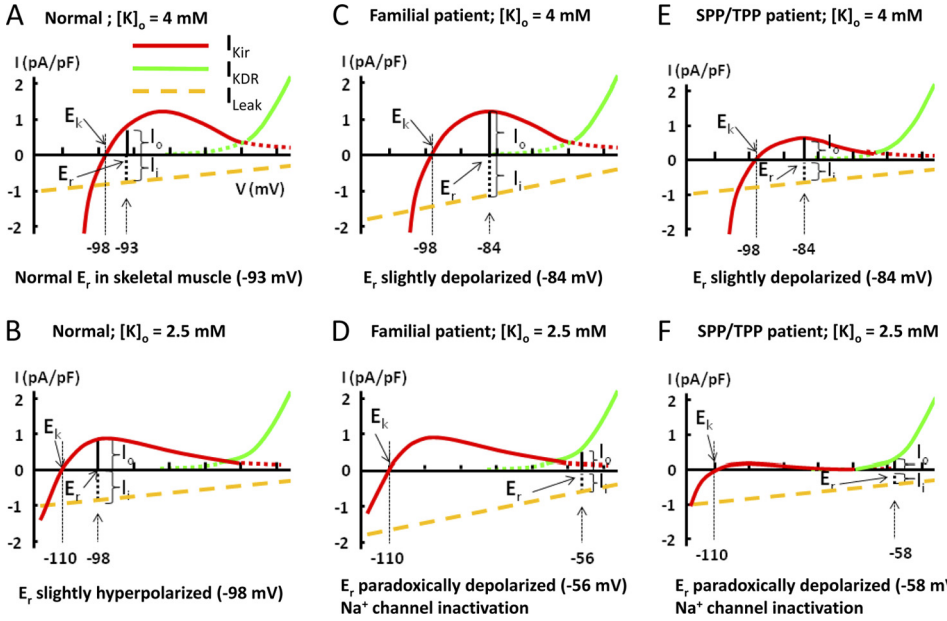

FIGURE 7. **Schematic models illustrating reduced outward current of Kir could induce paradoxical depolarization in patients with Kir2.6 mutation.** The steady-state current-voltage (*I-V*) relationship curve for K^+ current in mammalian skeletal muscle is a combination of *I-V* curves of inward rectifying K^+ channel (Kir, *red line*) and delayed rectifying K^+ channel (*KDR*, *green line*). Leakage current (*yellow dotted line*) has a reversal potential of 0 mV. Because gating pore currents from mutations of the voltage sensor only occur in hyperpolarized potentials, the inward leak current in familial hypoKPP patients is not linear (not illustrated here). The model is intended for conceptual understanding. The numerical value may be slightly different from the true *in vivo* value. See "Discussion" and Struyk and Cannon (19) for details. E_k, equilibrium potential of Kir channel; E_r, resting membrane potential; I_o, outward cation current; I_i, inward cation current; I_{Kir}, current of inward rectifying potassium channel; I_{KDR}, current of delayed rectifying potassium channel; I_{Leak}, inward cation leak current; $[K]_o$, extracellular potassium concentration.

7*A*). In the sarcolemma of skeletal muscle under most conditions, this balance occurs between the outward hump current of Kir (I_{Kir}) and inward cation leak current (I_{Leak}). Under some conditions, this balance can only be achieved by outward current mediated by the delayed rectifying K^+ channel (I_{KDR}), which is activated when membrane potentials depolarized to >-65 mV. These features give rise to the bi-stable distribution of resting membrane potentials of skeletal muscle sarcolemma. When extracellular K^+ concentration ($[K^+]_o$) decreases, the shift in the equilibrium potential for K^+ (E_k) toward hyperpolarized membrane potentials decreases the outward K^+ current through Kir relative to the leak current. In addition, decreased $[K^+]_o$ has a direct effect on Kir to reduce K^+ conductance (17, 18). As a result, the balance between inward and outward currents for E_r is reset to a hyperpolarized membrane potential (Fig. 7*B*; E_r −98 mV *versus* −93 mV in Fig. 7*A*). In normal individuals, unless the $[K^+]_o$ is extremely low (<1 mM), I_{Kir} is able to maintain the balance with I_{Leak} at hyperpolarized E_r. The ability to balance inward leak currents and I_{Kir} during hypokalemia by hyperpolarization of E_r is disrupted in familial hypoKPP. In the case of voltage-sensor mutations for $Ca_V1.1$ or $Na_V1.4$ channels in familial hypoKPP, the gating pore current increases in the leak current and causes a slight depolarization at normal $[K^+]_o$ (Fig. 7*C*). The hyperpolarizing shift in E_k in hypokalemia, however, renders imbalance between outward current mediated by Kir and the large inward leak current. As a result, E_r is reset to a more depolarized membrane potential where outward K^+ current is mediated by delayed rectifier K^+ channel in order to reach a new balance between outward and inward current (Fig. 7*D*).

The above model for hypokalemia-induced paradoxical depolarization predicts that reduced K^+ current through I_{Kir} could lead to the same effect as enhanced I_{Leak} (Fig. 7, *E* and *F*). This notion is supported by a recent study by Struyk and Cannon (19) showing that partial blockage of I_{Kir} by barium predisposes sarcolemma to the development of paradoxical depolarization under relatively normal $[K^+]_o$. Moreover, studies have shown that patients with non-familial hypoKPP and experimental models of TPP develop paradoxical depolarization under moderate hypokalemia despite no evidence of aberrant inward cation leak. Recordings from external intercostals muscle biopsied from TPP patients (20, 21) and hind limb muscle fibers of rat with hyperthyroidism (22) displayed persistently depolarized E_r. In the study of intercostals muscle of TPP patients, outward Kir currents were reduced along with diminished voltage-activated inward Na^+ currents (21). Our findings that mutations of Kir2.6 cause decreased outward K^+ currents through Kir2.6 and/or through Kir2.1 and Kir2.6 heteromultimeric channels support this model of hypokalemia-induced paradoxical depolarization and muscle inexcitability as a central mechanism of pathogenesis for paralysis in hypoKPP (Fig. 7, *E* and *F*). These findings may also explain why hypoKPP patients develop severe hypokalemia. Due to heterogeneity, muscle fibers develop paradoxical depolarization at different extracellular K^+ concentrations; the percentage of muscle fibers that develop paradoxical depolarization increases proportionally with decreasing $[K^+]_o$ (23). K^+ efflux across the sarcolemma (which is important for the extracellular K^+ homeostasis) at the paradoxically depolarized membrane potential is much lower than that in the normal resting membrane poten-

tial (compare Fig. 7, *D* and *F*, with Fig. 7*A*). Thus, an increase in the number of muscle fibers with paradoxical depolarization from the initial mild hypokalemia may set in motion a vicious positive feedback cycle of worsening hypokalemia by trapping K^+ in the myoplasm in the setting of paradoxical depolarization. The observation that hypokalemia and muscle paralysis develops in patients with barium intoxication supports this notion (19, 24).

Many members of Kir2.x family including Kir2.1, Kir2.2, and Kir2.6 are present in skeletal muscle (25). The subcellular distribution in the muscle and relative contribution of each member remain largely unknown. Some insights can be gained from human mutations and animal models. Mutations of Kir2.1 cause a multisystem disease featured by prolonged QT syndrome, facial and skeletal dysmorphism, and hypokalemic periodic paralysis known as Andersen-Tawil syndrome (26). The multiorgan involvement is consistent with the broad distribution of Kir2.1 in these and other organs (25). Mice homozygous for inactivation of Kir2.1 gene die at a young age due to palatal defects and difficulties in feeding (27). These findings indicate that Kir2.1 is essential for maintaining a normal E_r in cardiac and skeletal muscle as well as other tissues. Mice with knockout of Kir2.2 have no obvious phenotype (27). The report by Ryan *et al.* (12) and ours indicate an important role of Kir2.6 in the regulation of skeletal muscle membrane potentials. During the course of our present study, Dassau *et al.* (14) reported that Kir2.6 co-assembles with Kir2.1 and Kir2.2. Based on immunofluorescent staining of recombinant Kir2.6 in transfected rodent tissues, the authors suggested that Kir2.6 is predominantly distributed to the endoplasmic reticulum and functions as a dominant negative regulator of cell surface abundance of Kir2.x channels by retention in the endoplasmic reticulum. This mechanism, however, does not explain how mutations of Kir2.6 cause hypoKPP.

In this study we find that Kir2.6 expresses functional cell-surface current in a human cell line (HEK cells). Biotinylation assays confirm cell-surface expression of Kir2.6 channel (Fig. 3*B*). Ryan *et al.* (12) also observed functional expression in HEK cells. As acknowledged by Dassau *et al.* (14), different cell types may account for the apparent discrepancy. Moreover, we find that coexpression of Kir2.6 and Kir2.1 produces currents with mixed functional properties of Kir2.6 and Kir2.1 channel subunits, and disease Kir2.6 mutants exert dominant negative inhibition on Kir2.1. These results strongly indicate that the Kir2.6 channel expresses functional currents at the cell surface of human cells, and decreased outward K^+ currents through Kir2.6 and Kir2.1 (and perhaps other Kir channels as well) account for the pathogenesis of hypoKPP in patients with Kir2.6 mutations. Based on the observation that *KCNJ18* contains a thyroid-responsive element and thyroid hormone up-regulates the transcription of Kir2.6, Ryan *et al.* (12) suggested that up-regulation of Kir2.6 expression is important for mutant channel subunits to contribute to the pathogenesis of TPP. Indeed, as disease Kir2.6 mutants cause dominant negative inhibition of wild type Kir2.6 and Kir2.1, an increase in the cell-surface abundance of mutant subunits by thyroid hormone would enhance the decrease of functional K^+ currents in the sarcolemma. The base-line reduction of sarcolemma K^+ currents from mutations of Kir2.6 subunits, however, can lead to hypoKPP, as evident in SPP patients with normal levels of thyroid hormone. Future study will investigate subcellular distribution of Kir2.1 and Kir2.6, physiological significance of differential distribution, and the potential impact of disease mutants on homomeric and/or heteromeric subunits.

Ryan *et al.* (12) reported mutations of Kir2.6 ranging from 0 to 33% in TPP patients from several different populations. In our Taiwanese population, we found four mutations in 180 SPP and TPP patients. Mutations in $Ca_v1.1$, $Na_v1.4$, and Kir2.1 have not been reported in TPP (28–31). Mutations in $Ca_v1.1$ and $Na_v1.4$, however, have been reported in some SPP patients (Ref. 32; see also "Experimental Procedures"). These patients may be variants of familial hypoKPP due to an incomplete penetration of female carriers or may be afflicted by *de novo* gene mutations. Whether decreased protein expression and/or function of Kir2.6, promoter polymorphism, and/or deep intron mutations of *KCNJ18* may account for disease phenotypes in some of TPP and SPP patients not mapped to mutations of the coding region of Na^+, Ca^{2+}, and Kir2.6 channels awaits further investigation. Of note, insulin, of which an increased blood level is a predisposing factor for hypoKPP, was reported to inhibit Kir currents (33). In conclusion, our present report provides the first evidence that mutations in Kir2.6 occur in SPP as well as TPP, supporting the notion that decreased K^+ currents predispose the sarcolemma to paradoxical depolarization in hypokalemia leading to muscle paralysis.

REFERENCES

1. Stedwell, R. E., Allen, K. M., and Binder, L. S. (1992) *Am. J. Emerg. Med.* **10,** 143–148
2. Lin, S. H., Lin, Y. F., and Halperin, M. L. (2001) *QJM* **94,** 133–139
3. Ptácek, L. J., Tawil, R., Griggs, R. C., Engel, A. G., Layzer, R. B., Kwieciński, H., McManis, P. G., Santiago, L., Moore, M., and Fouad, G. (1994) *Cell* **77,** 863–868
4. Bulman, D. E., Scoggan, K. A., van Oene, M. D., Nicolle, M. W., Hahn, A. F., Tollar, L. L., and Ebers, G. C. (1999) *Neurology* **53,** 1932–1936
5. Matthews, E., Labrum, R., Sweeney, M. G., Sud, R., Haworth, A., Chinnery, P. F., Meola, G., Schorge, S., Kullmann, D. M., Davis, M. B., and Hanna, M. G. (2009) *Neurology* **72,** 1544–1547
6. Ober, K. P. (1992) *Medicine* **71,** 109–120
7. Lin, S. H. (2005) *Mayo Clin. Proc.* **80,** 99–105
8. Okinaka, S., Shizume, K., Iino, S., Watanabe, A., Irie, M., Noguchi, A., Kuma, S., Kuma, K., and Ito, T. (1957) *J. Clin. Endocrinol. Metab.* **17,** 1454–1459
9. Kelley, D. E., Gharib, H., Kennedy, F. P., Duda, R. J., Jr., and McManis, P. G. (1989) *Arch. Intern. Med.* **149,** 2597–2600
10. Shiang, J. C., Cheng, C. J., Tsai, M. K., Hung, Y. J., Hsu, Y. J., Yang, S. S., Chu, S. J., and Lin, S. H. (2009) *Eur. J. Endocrinol.* **161,** 911–916
11. Kung, A. W. (2006) *J. Clin. Endocrinol. Metab.* **91,** 2490–2495
12. Ryan, D. P., da Silva, M. R., Soong, T. W., Fontaine, B., Donaldson, M. R., Kung, A. W., Jongjaroenprasert, W., Liang, M. C., Khoo, D. H., Cheah, J. S., Ho, S. C., Bernstein, H. S., Maciel, R. M., Brown, R. H., Jr., and Ptácek, L. J. (2010) *Cell* **140,** 88–98
13. Lazrak, A., Liu, Z., and Huang, C. L. (2006) *Proc. Natl. Acad. Sci. U.S.A.* **103,** 1615–1620
14. Dassau, L., Conti, L. R., Radeke, C. M., Ptáček, L. J., and Vandenberg, C. A. (2011) *J. Biol. Chem.* **286,** 9526–9541
15. Sokolov, S., Scheuer, T., and Catterall, W. A. (2007) *Nature* **446,** 76–78
16. Struyk, A. F., and Cannon, S. C. (2007) *J. Gen. Physiol.* **130,** 11–20
17. Chang, H. K., Lee, J. R., Liu, T. A., Suen, C. S., Arreola, J., and Shieh, R. C. (2010) *J. Biol. Chem.* **285,** 23115–23125
18. Liu, T. A., Chang, H. K., and Shieh, R. C. (2011) *Biochim. Biophys. Acta* **1808,** 1772–1778

19. Struyk, A. F., and Cannon, S. C. (2008) *Muscle Nerve* **37,** 326–337
20. Gruener, R., Stern, L. Z., Payne, C., and Hannapel, L. (1975) *J. Neurol. Sci.* **24,** 339–349
21. Puwanant, A., and Ruff, R. L. (2010) *Muscle Nerve* **42,** 315–327
22. Hofmann, W. W., and Denys, E. H. (1972) *Am. J. Physiol.* **223,** 283–287
23. Jurkat-Rott, K., Weber, M. A., Fauler, M., Guo, X. H., Holzherr, B. D., Paczulla, A., Nordsborg, N., Joechle, W., and Lehmann-Horn, F. (2009) *Proc. Natl. Acad. Sci. U.S.A.* **106,** 4036–4041
24. Bowen, L. N., Subramony, S. H., Cheng, J., Wu, S. S., and Okun, M. S. (2010) *Neurology* **74,** 1546–1549
25. Hibino, H., Inanobe, A., Furutani, K., Murakami, S., Findlay, I., and Kurachi, Y. (2010) *Physiol. Rev.* **90,** 291–366
26. Plaster, N. M., Tawil, R., Tristani-Firouzi, M., Canún, S., Bendahhou, S., Tsunoda, A., Donaldson, M. R., Iannaccone, S. T., Brunt, E., Barohn, R., Clark, J., Deymeer, F., George, A. L., Jr., Fish, F. A., Hahn, A., Nitu, A., Ozdemir, C., Serdaroglu, P., Subramony, S. H., Wolfe, G., Fu, Y. H., and Ptácek, L. J. (2001) *Cell* **105,** 511–519
27. Zaritsky, J. J., Eckman, D. M., Wellman, G. C., Nelson, M. T., and Schwarz, T. L. (2000) *Circ. Res.* **87,** 160–166
28. Chen, L., Lang, D., Ran, X. W., Joncourt, F., Gallati, S., and Burgunder, J. M. (2003) *Eur. Neurol.* **49,** 227–230
29. Ng, W. Y., Lui, K. F., Thai, A. C., and Cheah, J. S. (2004) *Thyroid* **14,** 187–190
30. Schalin-Jantti, C., Laine, T., Valli-Jaakola, K., Lonnqvist, T., Kontula, K., and Valimaki, M. J. (2005) *Horm. Res.* **63,** 139–144
31. Wang, W., Jiang, L., Ye, L., Zhu, N., Su, T., Guan, L., Li, X., and Ning, G. (2006) *Mol. Genet. Metab.* **87,** 359–363
32. Lin, S. H., Hsu, Y. D., Cheng, N. L., and Kao, M. C. (2005) *Am. J. Med. Sci.* **329,** 66–70
33. Ruff, R. L. (1999) *Neurology* **53,** 1556–1563